Journal of Electronic Materials (2024) 53:312–321
https://doi.org/10.1007/s11664-023-10773-4

ORIGINAL RESEARCH ARTICLE

Electronic and Thermoelectric Properties of Yb^{2+}-Doped Cubic Perovskite $CsCaCl_3$: A First-Principles Study

Altaf Ur Rahman[1] · Rashid Khan[2] · Nawishta Jabeen[3] · Sajid Khan[4] · Yousef Mohammed Alanazi[5] · Muhammad Abdul[6]

Received: 28 May 2023 / Accepted: 5 October 2023 / Published online: 31 October 2023

Abstract

First-principles calculations are used to study the structural, electrical, and thermoelectric properties of pure and Yb^{2+}-doped $CsCaCl_3$ perovskite. Thermoelectric transport properties as a function of chemical potentials (μ), temperature (T), and Yb^{2+} dopant concentration (x) are computed using semi-classical Boltzmann theory implemented in the BoltzTrap code. The calculated indirect bandgap of pure $CsCaCl_3$ is 5.35 eV, and it behaves like an insulator. To tailor the electronic and thermoelectric properties of the $CsCaCl_3$ compound, we considered substitutional doping with the lanthanide Yb^{2+} atom for possible desired applications. According to the predicted formation energy, Yb^{2+}-doped at the cation site (Ca-site) is structurally more stable than at the anion site. Within the bandgap of pure $CsCaCl_3$, the Yb^{2+} dopant induces defective states. As a result, transitions from insulator to semiconductor and indirect to direct bandgap occurred. According to the partial density of states, the Yb^{2+} atom's *f*-orbital produced impurity states above the valance band maximum (VBM), resulting in a narrower bandgap. For both values of chemical potential (μ = conduction bad minimum [CBM] and VBM), we characterize the thermoelectric properties. Additionally, various Yb^{2+} dopant concentrations were taken into account. At μ = CBM, substitutional Yb^{2+} doping at a concentration level of 1.67% demonstrates an improvement in the thermoelectric properties. The highest ZT value for $CsCaCl_3$:Yb^{2+} 1.67% at μ = CBM is 1.4 at 1150 K. According to the ZT value, Yb^{2+}-doped $CsCaCl_3$ cubic perovskite compound can be used in thermoelectric applications.

Graphical Abstract

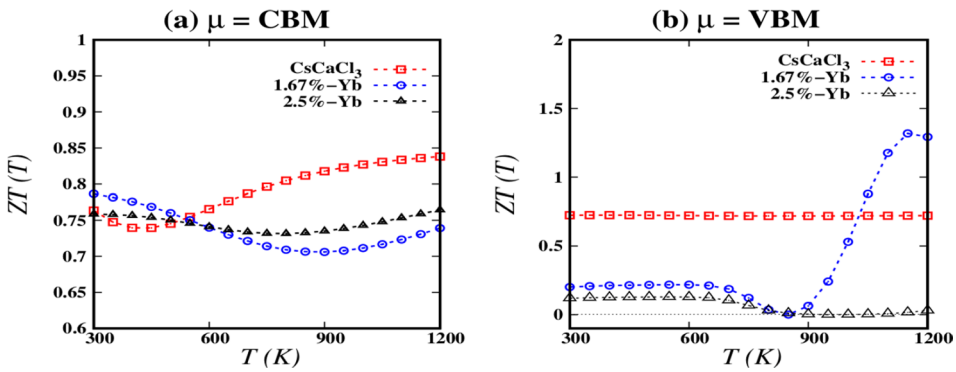

Keywords Perovskite materials · density functional theory · electronic properties · Boltzmann transport equations · thermoelectric properties

Extended author information available on the last page of the article

Introduction

The use of halide phosphors has increased significantly over the last few decades[1] due to its advantageous properties such as high light yield, fast decay, high energy resolution, and thermal stability. Phosphors are usually utilized in high-energy materials science, as a detector in medical diagnostics, in medical imaging, in LEDs to produce different colors, and in geophysical investigation, which drives researchers to build better phosphors for multiple applications. Many novel phosphor materials have been synthesized and used extensively over the years.[2,3] A single perovskite (ABX_3) is a ternary halide, where A represents a cation, B is a transition metal, and X is a halide. The family of perovskite ABX_3 compounds includes a variety of materials with huge bandgaps that can host dopants (lanthanoid series elements or transition metals)[4] to tune their electronic properties. Alemanyet et al. examined the crystal structure and electrical and optical properties of a variety of phosphor inorganic materials with broad bandgaps and proposed their use as host material for dopants.[5] Obodo et al.[6] studied the electrical and optical characteristics of HfS_2 monolayers substituted with lanthanoid series of elements.

According to the literature, broad-bandgap materials, such as $CsCaX_3$ (X: Cl, Br, I), are a possible series of candidate materials for substitutional doping with lanthanoid to tune their electrical and thermoelectric characteristics to match the needs of thermoelectric device applications. Grimm et al. experimentally synthesized a series of $CsCaX_3$ halide compounds by mixing the powders of CsX and CaX_2 in a stoichiometric ratio.[7] A stoichiometric ratio means that the amount of substance will react completely with the available amount of another reactant, with no extra amount of either substance. The increase in global energy consumption and the limited oil, gas, and coal resources have driven efforts to minimize energy usage and search for alternative materials to be used for green energy applications to fulfill energy needs in the current environment. Therefore, materials scientists are engineering the properties of materials for desired green energy applications. For example, recently, a commensurate TiO_2 /V_2 O_5 van der Waals heterostructure with a type II band alignment was proposed for potential application in photovoltaics, which was confirmed experimentally.[8,9] Similarly, high thermoelectric performance in both n-type and p-type CdSb materials is experimentally realized, which is the basic requirement for designing an efficient thermoelectric generator.[10]

For thermoelectric devices, we need thermoelectric materials, and the efficiency of thermoelectric materials is determined by different factors, including a high Seebeck coefficient (S), fast electrical and ionic conductivity (σ), low electronic thermal conductivity (κ_e), and low lattice thermal conductivity (κ_{lat}). This will result in a high figure of merit (ZT), which is often used to used to quantify the thermoelectric performance of the materials. Fast ionic conductivity was observed in halide-based perovskites at higher temperature, and halide vacancies are responsible for the fast ionic conductivity.[11] Recently, cesium (Cs)-based inorganic perovskites have attracted much attention due to their high thermal stability.[12] Ephraim Babu et al. studied the elastic and optical properties of $CsCaCl_3$.[13] The European Union has established restrictions for hazardous materials, including lead (Pb). As lead-free halide perovskites are recognized for their low toxicity and low cost, we decided to study the Yb^{2+}-doped $CsCaCl_3$ crystal structure and explore its electronic and thermoelectric properties. Pure $CsCaCl_3$ perovskite is a wide-bandgap material. For possible thermoelectric applications, we need to tune the bandgap to smaller values because a small bandgap is required for thermoelectric applications. For example, in the case of a narrow-bandgap material, electronic thermal excitation will occur very easily when heat is supplied. For this reason, we considered Yb^{2+} substitutional doping in the $CsCaCl_3$ crystal structure.

Thermal energy stored in thermoelectric materials can produce electrical energy from waste heat. Thus, thermoelectric materials can be employed as a green energy source[14–17] to produce electrical energy from waste heat.[18] Many perovskite materials have been investigated for their thermoelectric properties, and they appear to hold promise for use in thermal energy storage to generate electricity.[19,20] The choice of material for thermoelectric generators is determined by the ZT value, which determines its thermoelectric efficiency; i.e., $ZT \geq 1$ is an indication of good thermoelectric materials.[18] A higher ZT value indicates better efficiency of waste heat conversion into electricity.[21] The ZT is a dimensionless quantity and is defined as

$$ZT = \frac{\sigma S^2}{\kappa_1 + \kappa_e} T \tag{1}$$

where σ, S, κ_l, κ_e, and T stand for electrical conductivity, Seebeck coefficient, lattice thermal conductivity, electronic thermal conductivity, and temperature, respectively. For real thermoelectric applications, the $ZT \geq 1$ material is used. As a result, substantial effort has been devoted to enhancing the ZT value. Two alternatives for increasing the ZT value are to increase the thermopower (σS^2) or to reduce the heat conduction by phonons, known as phonon thermal conductivity (denoted as $\kappa_l at$).[18] In this work, motivated by the early promising use of transition metal oxides, the structural, electrical, and thermoelectric properties of perovskite are investigated. The main focus of this research is on the electronic

and thermoelectric characteristics of pure $CsCaCl_3$ and Yb^{2+}-doped $CsCaCl_3$ compounds at concentration levels of 1.67% and 2.5%. We first examined the structural and electronic characteristics of the pristine $CsCaCl_3$ compound. Next, by estimating the formation energy, we looked into the most stable dopant site for Yb^{2+}-doping in the $CsCaCl_3$ crystal structure. In addition, the effect of Yb^{2+}-doping on the structural, electrical, and thermoelectric properties of $CsCaCl_3$ was examined. These findings will aid experimentalists in the design and construction of good candidates for thermoelectric devices.

Computational Methodology

The Quantum ESPRESSO package,[22] which employs the plane wave pseudopotential to execute first-principles calculations based on density functional theory (DFT), was used for computations.[23] To determine the exchange and correlation interactions, the generalized gradient approximation (GGA+PBE) was used.[24] The pseudopotentials treat the valence electron configurations as follows: 1 for Cs:(Xe) + $6s^1$, 2 for Ca:(Ar) +$4s^2$, 7 for Cl:(Ne) +$3s^23p^5$, and 16 for Yb^{+2}:(Xe) +$4f^{14}6s^2$. In order to determine the electron wave function, optimal values for the wave function cutoff of 70 Ry and charge density cutoff of 300 Ry were used. For pure $CsCaCl_3$ compound, a primitive cell is used, while for substitutional doping we considered two supercells $2 \times 2 \times 2$ and $3 \times 2 \times 2$ to vary the dopant concentrations as shown in the Fig. 1a and b. The Monkhorst–Pack method[25] was used to sample *k*-meshes in the first Brillouin zone (BZ). All computational parameters were optimized. All structures were relaxed until the Hellmann–Feynman (HF) force on each atom was less than 0.003 Ry/Bohr. We used the BoltzTrap package, which is based on the semiclassical Boltzmann transport theory,[26] to calculate the thermoelectric properties as a function of temperature in the range of 300–1200 K and chemical potential (μ). A constant relaxation time based on the rigid band approximation is used to calculate the thermoelectric properties[26] of both pure and doped compounds. Thermoelectric transport coefficients are calculated from the analysis of the electronic band structure.[27,28] The details of Boltzmann transport calculations are given in our previous works.[29,30] The thermoelectric properties of different compounds were previously computed using the semiclassical Boltzmann equation within the constant relaxation time approximation.[31] The constant relaxation time approximation is based on the assumption that scattering time does not change significantly with energy. This approximation has previously been successful in predicting the thermoelectric characteristics of many materials.[32–34] This has been examined both experimentally and conceptually, and the results are highly accurate.[35] In the BoltzTrap code, constant relaxation time ($\tau = 10^{-14}$) is used in the computations for the thermoelectric properties.[26] In a recent study, the relaxation time ($\tau = 1.0\times10^{-14}$ s) was used to determine the thermoelectric properties of $CsPbBr_3$ and Rb-doped $CsPbBr_3$ compounds.[36] Therefore, in this study, the thermoelectric characteristics of pristine and Yb^{2+}-doped $CsCaCl_3$ with varied concentrations of 1.67% and 2.5% are investigated as a function of temperature in the range of 300–1200 K and chemical potential . The electrical and thermal conductivities are represented by $\left(\frac{\sigma}{\tau}\right)$ and $\left(\frac{\kappa}{\tau}\right)$, respec-

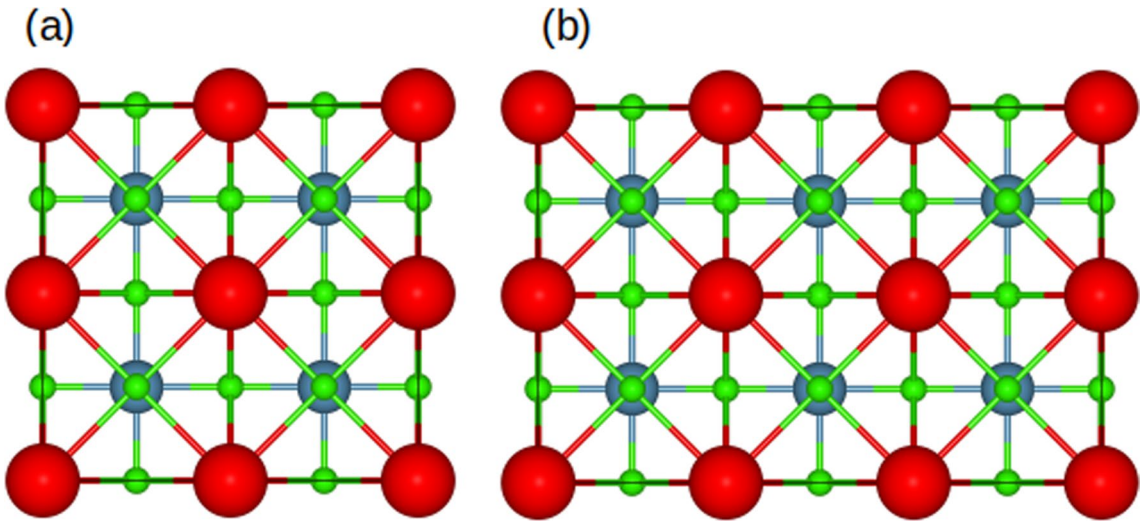

Fig. 1 Schematic top view representation of $CsCaCl_3$ (a) supercell with dimensions $2 \times 2 \times 2$ used for Yb^{2+} dopant concentration of 2.5%, and (b) supercell with dimensions $3 \times 2 \times 2$ used for Yb^{2+} dopant concentration of 1.67%. The Cs, Ca, and Cl atoms are represented by the red, blue, and green spheres, respectively (Color figure online).

tively. The electronic conductivity (κ_e) is added to the lattice thermal conductivity (κ_l) to obtain the total thermal conductivity: $\kappa = \kappa_e + \kappa_l$. The κ_e is a more dominant factor than the κ_l in κ, so the BoltzTrap code is used to calculate the κ_e while treating the κ_l as a constant.[30]

Results and Discussion

Structural and Electronic Properties

The cubic crystal structure of $CsCaCl_3$ (#221) belongs to the space group $P-3m$. Three Cl atoms are situated on the cube's adjacent faces, one Cs atom is in the cube's corner, and one Ca atom is in the body's center. These five atoms come together to form the $CsCaCl_3$ primitive unit cell. Atomic positions for Cs, Ca, and Cl are (0, 0, 0), (0.5, 0.5, 0.5), and (0.5, 0, 0.5), respectively.[1,4] The optimal lattice constant of pure $CsCaCl_3$ determined using GGA+PBE was 5.44, which is in good accord with the experimental evidence that is currently available[37] and earlier theoretical findings.[4] Using the optimized lattice parameter of pure $CsCaCl_3$, we construct two types of a supercells with dimensions of $2\times2\times2$ (see Fig. 1a) and dimensions of $3\times2\times2$ (see Fig. 1a) for different Yb^{2+} dopant concentrations. Figure 1a has a total of 40 atoms, among which one host atom is replaced by a Yb^{2+} atom, so the dopant concentration is 2.5%. Similarly, Fig. 1b has a total of 60 atoms, among which one host atom is substituted by a Yb^{2+} ion, so the dopant concentration is 1.67%. For the possible dopant sites (Cs-site, Ca-site, and Cl-site), we calculated the formation energy. The calculated formation energies are −0.45 eV, −3.23 eV, and −0.70 eV for Yb^{2+} doped at the Cs-site, Ca-site, and Cl-site, respectively. These results indicate that Yb^{2+} doped at the Ca-site is the most stable site. At the ground state, Yb^{2+} (divalent lanthanide) has a full-shell $4f^{14}$ structure. Yb^{2+} has parity-allowed transitions from the $4f$ ground state to the $5d$ excited state, and it can be used to tune the optical spectra of different host substances.[38] At the ground state, there are no unpaired electrons in the Yb^{2+}-doped $CsCaCl_3$ halide perovskite crystal structure; as a result, according to Hund's rule, we can predict no magnetization.[39] For further electronic and thermoelectric investigations, we considered Yb^{2+} doped at the Ca-site in the $CsCaCl_3$ supercell with varied concentrations 1.67% and 2.5% and performed non-spin polarization calculations. Since Yb^{2+} has an electronic configuration of $4f146s^2$, when Yb^{2+} ions are substituted at the Ca^{2+} site it remains closed shell and nonmagnetic, so it is not surprising that no spin polarization is observed by varying the dopant concentration. The electronic band structure of pristine $CsCaCl_3$, $CsCaCl_3$:Yb_{2+} (1.67%), and $CsCaCl_3$:Yb_{2+} (2.5%) is shown in Fig. 2a, b and c.

The predicted bandgap of pristine $CsCaCl_3$ is 5.35 eV (M–Γ) (see Fig. 2a), which is consistent with prior research.[4] The character of the bandgap of pure $CsCaCl_3$

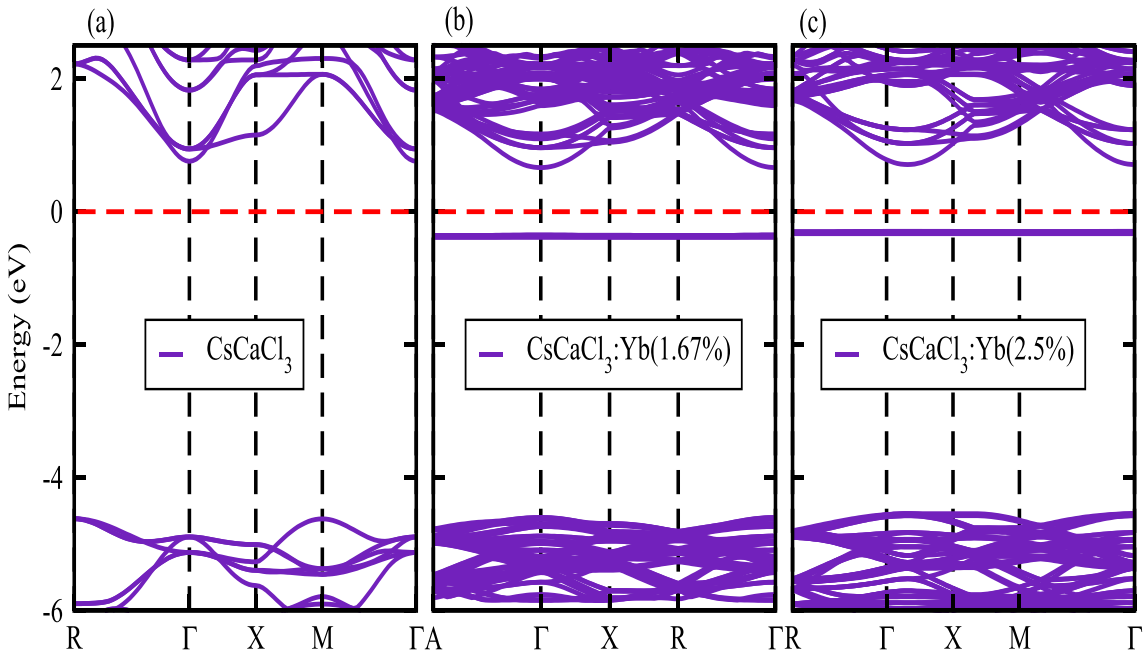

Fig. 2 The electronic band structure of (a) pristine $CsCaCl_3$, (b) $CsCaCl_3$:Yb^{2+} (1.67%), and (c) $CsCaCl_3$:Yb^{2+} (2.5%). The Fermi level at zero energy is represented by the horizontal dashed red line (Color figure online).

is changed from indirect to direct with Yb_{2+} doping. The defect states produced by Yb_{2+} dopants within the bandgap energy window result in the reduced bandgap. The $CsCaCl_3$:Yb^{2+} (1.67%) and $CsCaCl_3$:Yb^{2+} (2.5%) compounds have an electronic bandgap of 1.0 eV and 1.02 eV with respect to the defective state lies below the Fermi energy level, respectively. Interestingly, Yb^{2+} doping in the $CsCaCl_3$ compound results in the transition from an indirect to a direct bandgap (see Fig. 2b and c), which results in enhanced electronic characteristics. The pristine valence band maximum (VBM) consists of the major (minor) contribution of *p*-orbital states of Cl and Cs atoms, whereas the conduction band minimum (CBM) is formed by the prominent (subsidiary) contribution of *d* (*p*)-orbital states of the Cs atom. The PDOS of $CsCaCl_3$:Yb^{2+} (1.67%) is shown in Fig. 3d, e and f, and the defective states below the Fermi level are formed due to the significant (small) contribution of *f* (*p*)-orbital states of the Yb^{2+} (Cl) atom. Figure 3g, h, and i demonstrate the PDOS of $CsCaCl_3$:Yb^{2+} (2.5%). It follows the same trend in electronic properties, i.e, the PDOS of orbitals' contribution at various states is the same as in the previous situation.

Thermoelectric Properties

In this section, the thermoelectric properties for the pristine $CsCaCl_3$ and Yb^{2+}-doped $CsCaCl_3$ at the most stable site (Ca-sites) with varied concentration levels of 1.67% and 2.5% are examined. These properties include electrical conductivity σ, Seebeck coefficient *S*, electronic thermal conductivity κ, power factor *PF*, and figure of merit *ZT* as a function of temperature in the range of 300–1200 K, and chemical potential μ = CBM (at the left side of Figs. 4, 5, and 6) and μ VBM (at the right side of Figs. 4, 5, and 6). The electronic conductivity at both chemical potentials is presented in Fig. 4a and d, Seebeck coefficient in Fig. 4b and e, and thermopower PF in Fig. 4c and f. The thermoelectric capabilities of the pristine and Yb^{2+}-doped $CsCaCl_3$

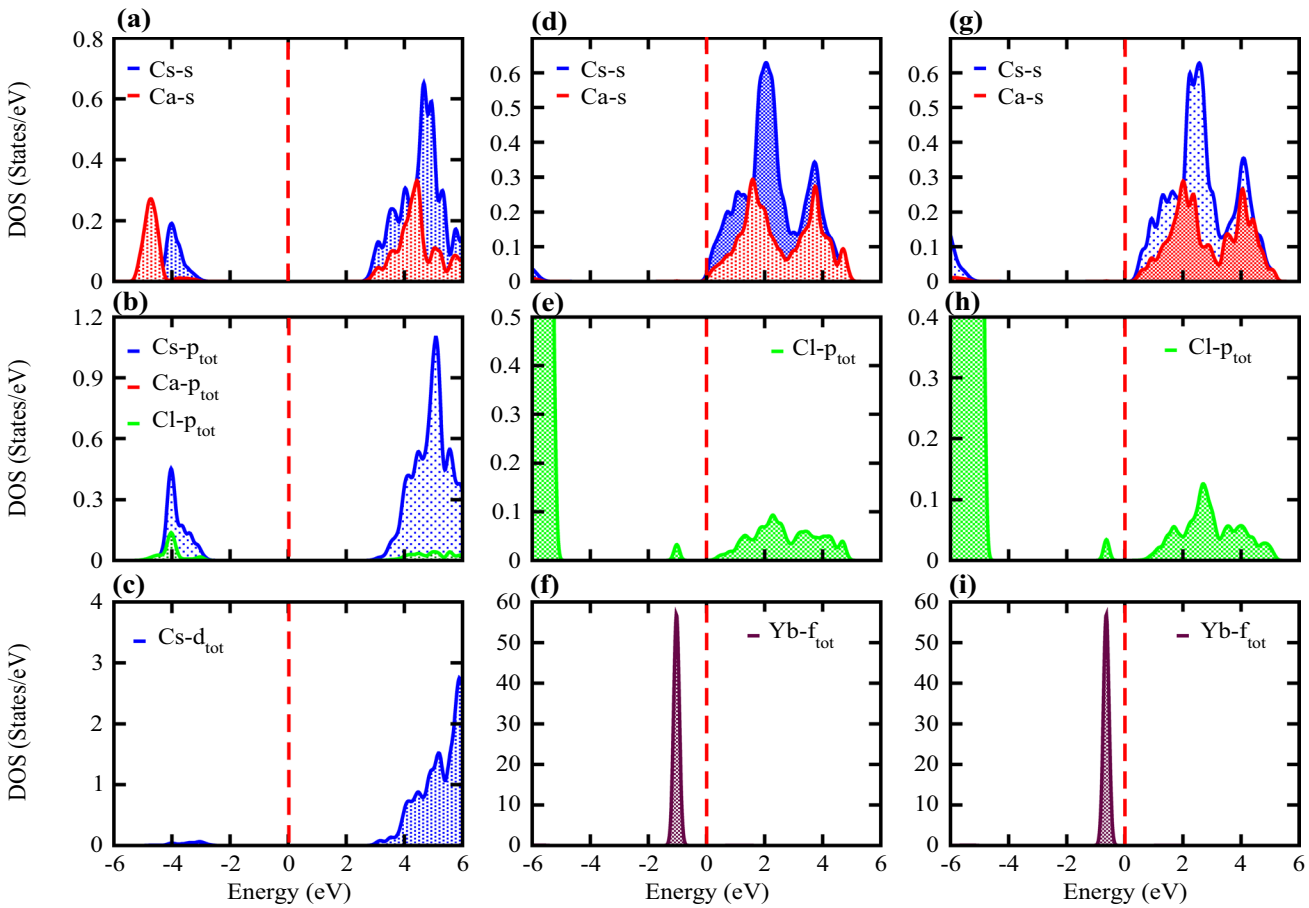

Fig. 3 Partial density of states (PDOS) (a–c) of pristine $CsCaCl_3$, (d–f) of $CsCaCl_3$:Yb^{2+} (1.67%), and (g–i) of $CsCaCl_3$:Yb^{2+} (2.5%). The PDOS of Cs, Ca, Cl, and the dopant Yb^{2+} atoms are represented by blue, red, green, and maroon colors, respectively. The Fermi level at zero energy is represented by the horizontal dashed red line (Color figure online).

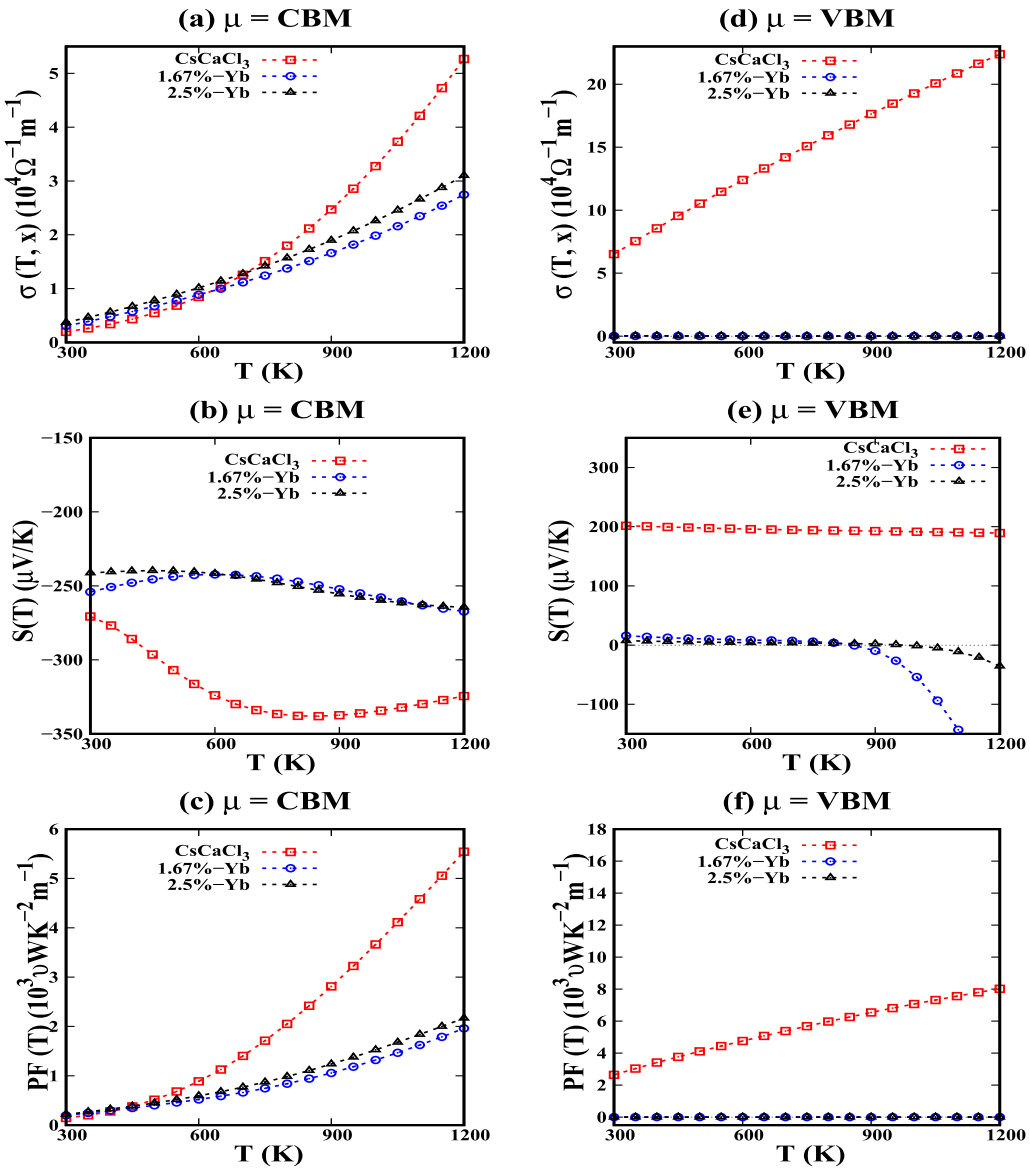

Fig. 4 GGA+PBE calculated thermoelectric characteristics of pure $CsCaCl_3$ and Yb^{2+}-doped $CsCaCl_3$ at Ca-sites with dopant concentration levels of 1.67% and 2.5% as a function of temperature (T) at a chemical potential (μ) equal to minimum energy of the conduction band (a–c) left panel, and μ equal to energy of the valance band maximum (d–f) right panel (Color figure online).

compounds with concentration levels of 1.67% and 2.5% are represented by the red, blue, and black colors, respectively. Figure 4a and d illustrate the electrical conductivity of pristine $CsCaCl_3$ and Yb_{2+}-doped $CsCaCl_3$ at Ca-sites with dopant concentration levels of 1.67% and 2.5% as a function of temperature and chemical potential. Setting the chemical potential μ equal to the energy of the conduction band maxima (CBM), the electrical conductivity (σ) of pristine $CaCaCl_3$ increases with temperature and dopant concentration up to 700 K (see Fig. 4a). At a temperature higher than 700 K, the electrical conductivity decreases with Yb_{2+} dopant in $CsCaCl_3$ at Ca-sites (see Fig. 4). This is due to the fact that at higher temperatures, electrons were more scattered with dopants, which results in reduced electrical conductivity. Similarly, setting the chemical potential μ equal to the energy of the valence band maxima (VBM), the electrical conductivity is calculated (see Fig. 4d). The electrical conductivity $_{\sigma}$ of pure $CsCaCl_3$ increases with temperature while the electrical conductivity ($_{\sigma}$) of Yb^{2+}-doped $CsCaCl_3$ at Ca-sites is approximately constant with temperature.

The Seebeck coefficient (S) of pure $CsCaCl_3$ and Yb_{2+}-doped $CsCaCl_3$ at Ca-sites with concentration levels of 1.67% and 2.5% is plotted as a function of temperature in Fig. 4b and e. The values of S are negative in all cases, with the greatest value of S being around $-340\ \mu V/K$ in pure

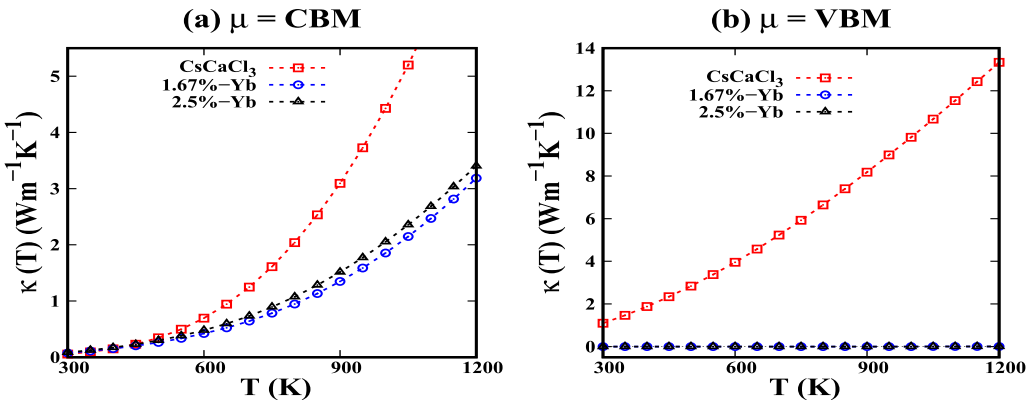

Fig. 5 Electronic conductivity (κ) of pristine $CsCaCl_3$ and Yb^{2+}-doped $CsCaCl_3$ at Ca-sites with concentration levels of 1.67% and 2.5% computed by GGA+PBE as a function of temperature and electronic chemical potential (a) μ = CBM (left panel) and (b) μ = VBM (right panel). The thermoelectric properties of the pristine and Yb^{2+}-doped $CsCaCl_3$ at Ca-sites with concentration levels of 1.67% and 2.5%, are represented by the red, blue, and black colors, respectively (Color figure online).

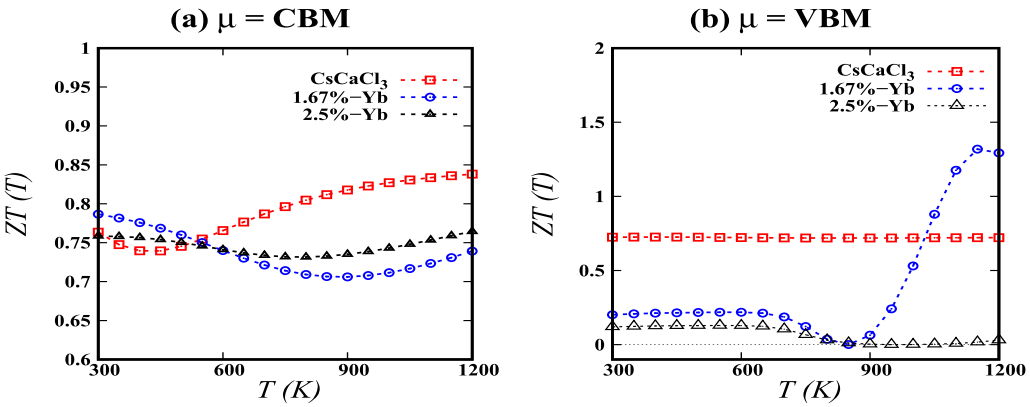

Fig. 6 GGA+PBE calculated thermoelectric properties of pristine and Yb^{2+}-doped $CsCaCl_3$ compounds as a function of T and μ (a) $ZT(T)$ left panel μ = CBM and (b) $ZT(T)$ right panel μ = VBM at concentration levels of 1.67% and 2.5%, respectively. The thermoelectric properties of the pristine and Yb^{2+}-doped $CsCaCl_3$ compounds with dopant concentration levels of 1.67% and 2.5% are represented by the red, blue, and black colors, respectively (Color figure online).

$CsCaCl_3$, as shown in Fig. 4b. Figure 4e demonstrates that for pure $CsCaCl_3$, the Seebeck coefficient S remains constant with temperature, whereas for the other two cases, it drops with temperature. While the greatest value of S for pure $CsCaCl_3$ is around $200 \mu V/K$ at μ = VBM, the maximum value of S for Yb_{2+}-doped $CsCaCl_3$ at a concentration level of 1.67% declines with rising temperature. According to the literature, the minimum requirements for thermoelectric materials to be used in practical applications are $S \geq 200$ $\mu V/K$.[40]

Figure 4c and f show the thermopower (PF = σS^2) of pure $CsCaCl_3$ and Yb_{2+}-doped $CsCaCl_3$ at Ca-sites with concentration levels of 1.67% and 2.5%. In all three compounds, the PF increases as the temperature rises. In addition, at μ = CBM, the PF of pure $CsCaCl_3$ is higher than Yb_{2+}-doped $CsCaCl_3$. As shown in Fig. 4f, the PF of pure $CsCaCl_3$ increases with temperature at μ = VBM, but the PF of Yb_{2+}-doped $CsCaCl_3$ at Ca-sites with concentrations of 1.67% and 2.5% is nearly constant with temperature. Electronic thermal conductivity (κ_e) as a function of temperature and μ at equilibrium lattice constant is shown in Fig. 5a and b. There have been studies in the literature that overlook the lattice thermal conductivity and focus solely on the electronic part of thermal conductivity (e.g., see Refs.[41–43]). Increased temperature increases the electrical thermal conductivity. In thermoelectric devices, electrons absorb more photons at higher temperatures and shift from high to lower energy levels. As shown in Fig. 2b, the thermal conductivity of pure $CsCaCl_3$ increases with temperature at μ = VBM, but the thermal conductivity of Yb^{2+}

-doped $CsCaCl_3$ at Ca-sites with concentration levels of 1.67% and 2.5% remains constant with temperature.

Figure 6a and b show the *ZT* values for the pristine and Yb_{2+}-doped $CsCaCl_3$ samples as a function of temperature and μ. As a result, the *ZT* contains information about how efficient the material is for thermoelectric applications. Thermoelectric characteristics were calculated by varying the temperature while keeping the chemical potential constant. To investigate the material's *n*-type (*p*-type) behavior due to electron (hole) doping, we use two values of chemical potential (μ) equal to the energy of the CBM and VBM. According to our DFT calculations, Yb^{2+}-doped $CsCaCl_3$ behaves like a semiconductor at dopant concentration levels of 1.67% and 2.5%. The *n*-type and *p*-type carrier doping in a semiconductor can be investigated using rigid band approximation. As a result, the Fermi energy level shifts to the CBM and VBM by electron and hole doping, respectively. In the case of *p*-type thermoelectric performance, the highest *ZT* of the Yb^{2+}-doped $CsCaCl_3$ at Ca-sites with a concentration level of 1.67% is 1.4. This higher *ZT* value is due to the improved value of the Seebeck coefficient at higher temperatures. The Seebeck coefficient is proportional to the effective mass of the carriers.[20] The doping results in a flat band at the Γ point, which results in higher effective mass of the hole.

Regarding the *ZT* value, it was reported previously that for Cs-based fluoro-perovskite compounds, the values of *ZT* at room temperature are 0.56, 0.57, and 0.64 for $CsGeF_3$, $CsSnF_3$, and $CsPbF_3$, respectively.[36] Compared to oxide-based perovskites, this is substantially higher than theoretically[44] and experimentally[42] determined values for $SrTiO_3$. Thus, materials with *ZT* values greater than 1 can be considered candidate materials for thermoelectric applications. Figure 6a shows how the value of *ZT* for the pristine $CsCaCl_3$ at μ = CBM increased with temperature across a range of 500–1200 K, reaching its maximum value at 1200 K. Figure 6b depicts the *ZT* at the VBM, in which the *ZT* value of Yb^{2+}-doped $CsCaCl_3$ at Ca-sites with a concentration level of 1.67% remains constant in the temperature range of 300–650 K, decreases with temperature in the range of 650–900 K, and abruptly increases in the temperature range of 900–1200 K, reaching a maximum value of 1.4 at 1150 K, as shown in Fig. 3b. According to our DFT calculations, doping of Yb^{2+} in $CsCaCl_3$ at a concentration level of 1.67% improves the hole conduction (*p*-type); i.e., at temperatures greater than room temperature, the highest *ZT* value is reached at μ = VBM.

Conclusion

In this study, we examined the electrical and thermoelectric characteristics of pure and Yb^{2+}-doped $CsCaCl_3$ crystal structures via DFT implemented in Quantum ESPRESSO code in conjunction with BoltzTrap code. We examined the Yb^{2+} substitutional doping at the cation and anion sites in the $CsCaCl_3$ compound. The calculated formation energy indicates that the cation site is more stable than the anion site. Phosphor materials have a wide bandgap; pure $CsCaCl_3$ is an indirect-wide-bandgap phosphor compound with a bandgap of 5.4 eV. The phosphor material $CsCaCl_3$ is a good candidate for substitutional doping with lanthanide atoms for tuning electronic and thermoelectric properties. The dopant atom causes impurity states in the bandgap energy window of pure $CsCaCl_3$, resulting in a reduced bandgap. As a result, an insulator-to-semiconductor transition and indirect-to-direct bandgap transition occur. In this work, the transport characteristics of pure and Yb^{2+}-doped $CsCaCl_3$ were demonstrated as a function of chemical potential values (μ). The *n*-type doping caused by the Yb^{2+} doping results in a Seebeck coefficient greater than 200μV/K, which meets the conditions for thermoelectric materials to be employed in practical applications, which require S to be greater than 200μV/K. At μ = CBM and μ = VBM for both concentration levels, the electronic thermal conductivity of Yb^{2+}-doped $CsCaCl_3$ is reduced to lower values. As a result, in the situation where μ = CBM, we found an enhanced *ZT* value at room temperature. In contrast, we found that the maximal *ZT* value for $CsCaCl_3$:Yb^{2+} (1.67%) at μ = VBM is 1.4 at 1150 K. The increased *ZT* value indicates that the Yb^{2+}-doped $CsCaCl_3$ phosphor material is an appropriate candidate for thermoelectric applications.

Acknowledgments We acknowledge the Super-Computing facility at Ghulam Ishaq Khan Institute of Engineering Sciences and Technology funded by the Directorate of Science and Technology (DoST), Government of Khyber Pakhtunkhwa, and National Center for Physics (NCP) Islamabad, Pakistan. This work was supported in part by Oracle Cloud credits and related resources provided by the Oracle for Research program (Award Number CPQ-2652238). The authors would like to acknowledge Researcher's Supporting Project Number (RSP2023R511), King Saud University, Riyadh, Saudi Arabia.

Data Availability The data that support the findings of this study are available from the corresponding author upon reasonable request.

Conflict of interest We have no conflict of interest for this work to be declared.

References

1. A.H. Larbi, S. Hiadsi, M. Hadjab, and M. Saeed, 1-optical study of cubic, and orthorhombic structures of $XCaCl_3$(X= K, Rb) compounds: comparative Ab initio calculations. *Optik* 166, 169 (2018).
2. S. Derenzo, G. Bizarri, R. Borade, E. Bourret-Courchesne, R. Boutchko, A. Canning, A. Chaudhry, Y. Eagleman, G. Gundiah, and S. Hanrahan et al., 2-new scintillators discovered by high-throughput screening. *Nucl. Instrum. Methods Phys. Res. Sect. A Accel. Spectrom. Detect. Assoc. Equip.* 652(1), 247 (2011).

3. M. Tyagi, M. Zhuravleva, and C. Melcher, 3-theoretical and experimental characterization of promising new scintillators: Eu^{2+} doped $CsCaCl_3$ and $CsCaI_3$. *J. Appl. Phys.* 113(20), 203504 (2013).
4. K.E. Babu, N. Murali, K.V. Babu, P.T. Shibeshi, and V. Veeraiah, 4-structural, elastic, electronic, and optical properties of cubic perovskite $CsCaCl_3$ compound: an ab initio study. *Acta Phys. Pol. A* 125(5), 1179 (2014).
5. P. Alemany, I.P.R. de Moreira, R. Castillo, and J. Llanos, 5-electronic, structural, and optical properties of host materials for inorganic phosphors. *J. Alloy. Compd.* 513, 630 (2012).
6. K. Obodo, G. Gebreyesus, C. Ouma, J. Obodo, S. Ezeonu, D. Rai, and B. Bouhafs, 6-controlling the electronic and optical properties of HfS_2 mono-layers via lanthanide substitutional doping: a DFT+U study. *RSC Adv.* 10(27), 15670 (2020).
7. J. Grimm, J.F. Suyver, E. Beurer, G. Carver, and H.U. Güdel, 8-light-emission and excited-state dynamics in Tm^{2+} doped $CsCaCl_3$, $CsCaBr_3$, and $CsCaI_3$. *J. Phys. Chem. B* 110(5), 2093 (2006).
8. H. Ullah, A.U. Rahman, E.L. Aragão, F.F.A. Barbosa, K.G.R. Pergher, R. Giulian, H.C. Júnior, R.L. Sommer, and S. Khan, Homogeneous v incorporation via single-step anodization: structural doping or heterostructure formation? *Appl. Surf. Sci.* 556, 149694 (2021).
9. A.U. Rahman, J.M. Morbec, G. Rahman, and P. Kratzer, Commensurate versus incommensurate heterostructures of group-iii monochalcogenides. *Phys. Rev. Mater.* 2(9), 094002 (2018).
10. P. Zhao, H. Yao, S. Zhi, X. Ma, Z. Wu, Y. Liu, X. Wang, L. Yin, Z. Zhang, and S. Hou et al., Realizing n-type cdsb with promising thermoelectric performance. *J. Mater. Sci. Technol.* 144, 54 (2023).
11. A. Chadwick, J. Strange, G.A. Ranieri, and M. Terenzi, Studies of ionic motion in perovskite fluorides. *Solid State Ion.* 9, 555 (1983).
12. G.S. Perry and K.N. Moody, Cscl-$CaCl_2$ phase diagram. *Thermochim. Acta* 198(1), 167 (1992).
13. K. Ephraim Babu, N. Murali, K. Vijaya Babu, P. Taddesse Shibeshi, and V. Veeraiah, Structural, elastic, electronic, and optical properties of cubic perovskite $CsCaCl_3$ compound: an ab initio study. *Acta Phys. Pol. A* 125(5), 1179 (2014).
14. G.J. Snyder and E.S. Toberer, Complex thermoelectric materials, Materials for sustainable energy: a collection of peer-reviewed research and review articles from Nature Publishing Group (2011) 101.
15. B.G. Levi, Simple compound manifests record-high thermoelectric performance. *Phys. Today* 67(6), 14 (2014).
16. X. Zhang and L.-D. Zhao, Thermoelectric materials: energy conversion between heat and electricity. *J. Mater.* 1(2), 92 (2015).
17. A.D. LaLonde, Y. Pei, H. Wang, and G.J. Snyder, Lead telluride alloy thermoelectrics. *Mater. Today* 14(11), 526 (2011).
18. A.M. Dehkordi, M. Zebarjadi, J. He, and T.M. Tritt, Thermoelectric power factor: enhancement mechanisms and strategies for higher performance thermoelectric materials. *Mater. Sci. Eng. R. Rep.* 97, 1 (2015).
19. W.M. Khan, A.U. Rahman, M. Tufail, M. Ibrar, W.H. Shah, W.A. Syed, and B. Gul, Toward controlled thermoelectric properties of Pb and Sb co-doped nanostructured Thallium Telluride for energy applications. *Mater. Res. Express* 7(10), 105010 (2020).
20. M. Tufail, A.U. Rahman, B. Gul, W. Akram, H. Ullah, M.W. Iqbal, S.M. Ramay, and W.H. Shah, Effect of Pb doping on electronic and thermoelectric properties of thallium antimony telluride ($Tl_{8.33}Sb_{1.67-x}Pb_xTe_6$) nano-compound: a combined experimental and theoretical investigations. *Phys. B Condens. Matter.* 608, 412789 (2021).
21. H.J. Goldsmid et al., *Introduction to Thermoelectricity*, Vol. 121 (Springer, 2010).
22. P. Giannozzi, S. Baroni, N. Bonini, M. Calandra, R. Car, C. Cavazzoni, D. Ceresoli, G.L. Chiarotti, M. Cococcioni, and I. Dabo et al., QUANTUM ESPRESSO: a modular and open-source software project for quantum simulations of materials. *J. Phys. Condens. Matter.* 21(39), 395502 (2009).
23. W. Kohn and L.J. Sham, Self-consistent equations including exchange and correlation effects. *Phys. Rev.* 140(4A), A1133 (1965).
24. J.P. Perdew, K. Burke, and M. Ernzerhof, Generalized gradient approximation made simple. *Phys. Rev. Lett.* 77(18), 3865 (1996).
25. H.J. Monkhorst and J.D. Pack, Special points for Brillouin-zone integrations. *Phys. Rev. B* 13(12), 5188 (1976).
26. G.K. Madsen and D.J. Singh, BoltzTraP. A code for calculating band-structure dependent quantities. *Comput. Phys. Commun.* 175(1), 67 (2006).
27. J.M. Ziman, *Electrons and Phonons: The Theory of Transport Phenomena in Solids* (Oxford University Press, 2001).
28. W. Jones and N.H. March, *Theoretical Solid State Physics*, Vol. 35 (Courier Corporation, 1985).
29. A.U. Rahman, A. Jamil, S. Khan, M. Ibrar, I. Ullah, R. Ahmad, and A. Dahshan, First-principles computational exploration of thermoelectric properties of bulk-gan and monolayer-gan. *J. Electron. Mater.* 51(6), 3317 (2022).
30. A.U. Rahman, M. Aurangzeb, R. Khan, Q. Zhang, and A. Dahshan, Predicted double perovskite material ca2zrtio6 with enhanced n-type thermoelectric performance. *J. Solid State Chem.* 305, 122661 (2022).
31. T. Thonhauser, T. Scheidemantel, J. Sofo, J. Badding, and G. Mahan, Thermoelectric properties of Sb_2Te_3 under pressure and uniaxial stress. *Phys. Rev. B* 68(8), 085201 (2003).
32. J. Sun and D.J. Singh, Thermoelectric properties of n-type $SrTiO_3$. *APL Mater.* 4(10), 104803 (2016).
33. S. Bhattacharyya, T. Pandey, and A.K. Singh, Effect of strain on electronic and thermoelectric properties of few layers to bulk MoS_2. *Nanotechnology* 25(46), 465701 (2014).
34. I. Bejenari and V. Kantser, Thermoelectric properties of bismuth telluride nanowires in the constant relaxation-time approximation. *Phys. Rev. B* 78(11), 115322 (2008).
35. J.U. Rahman, W.H. Nam, N. Van Du, G. Rahman, A.U. Rahman, W.H. Shin, W.-S. Seo, M.H. Kim, and S. Lee, Oxygen vacancy revived phonon-glass electron-crystal in srtio3. *J. Eur. Ceram. Soc.* 39(2–3), 358 (2019).
36. E. Ouaaka, M. Aazza, A. Bouymajane, and F. Cacciola, Electronic, optical, thermoelectric and elastic properties of rbxcs1-xpbbr3 perovskite. *Molecules* 28(7), 2880 (2023).
37. R.L. Moreira and A. Dias, Comment on "prediction of lattice constant in cubic perovskites." *J. Phys. Chem. Solids* 68(8), 1617 (2007).
38. M. Suta and C. Wickleder, 7-spin crossover of Yb^{2+} in $CsCaX_3$ and $CsSrX_3$ (X= Cl, Br, I)–A guideline to novel halide-based scintillators. *Adv. Funct. Mater.* 27(2), 1602783 (2017).
39. R. Khan, K.U. Rahman, Q. Zhang, A.U. Rahman, S. Azam, and A. Dahshan, The effect of substitutional doping of yb^{2+} on structural, electronic, and optical properties of $CsCaX_3$(X: Cl, Br, I) phosphors: a first-principles study. *J. Phys. Condens. Matter.* 34(6), 065502 (2021).
40. M. Zahedifar and P. Kratzer, Band structure and thermoelectric properties of half-heusler semiconductors from many-body perturbation theory. *Phys. Rev. B* 97(3), 035204 (2018).
41. J. Hong, C. Lee, J.-S. Park, and J.H. Shim, Control of valley degeneracy in MoS_2 by layer thickness and electric field and its effect on thermoelectric properties. *Phys. Rev. B* 93(3), 035445 (2016).
42. K. Ozdogan, M. Upadhyay Kahaly, S. Sarath Kumar, H.N. Alshareef, and U. Schwingenschlögl, Enhanced carrier density in

Nb-doped $SrTiO_3$ thermoelectrics. *J. Appl. Phys.* 111(5), 054313 (2012).
43. A. Ali, A.U. Rahman, and G. Rahman, Thermoelectric properties of $KCaF_3$. *Phys. B Condens. Matter.* 565, 18 (2019).
44. G. Rahman and A.U. Rahman, Thermoelectric properties of n and p-type cubic and tetragonal $XTiO_3$(X= Ba, Pb): a density functional theory study. *Phys. B Condens. Matter.* 526, 122 (2017).

Authors and Affiliations

Altaf Ur Rahman[1] · Rashid Khan[2] · Nawishta Jabeen[3] · Sajid Khan[4] · Yousef Mohammed Alanazi[5] · Muhammad Abdul[6]

✉ Altaf Ur Rahman
altaf.urrahman@riphah.edu.pk

Rashid Khan
khan.rashid@stu.xjtu.edu.cn

[1] Department of Physics, Riphah International University, Lahore, Pakistan

[2] School of Energy and Power Engineering, Xi'an Jiaotong University (XJTU), 28 Xianning W. Rd, Xi'an 710049, China

[3] Department of Physics, Fatima Jinnah Women University Rawalpindi, Rawalpindi 46000, Pakistan

[4] Department of Physics, KUST, Kohat, KPK, Pakistan

[5] Chemical Engineering Department, College of Engineering, King Saud University Riyadh, Riyadh, Saudi Arabia

[6] School of Integrated Circuit Science and Engineering, University of Electronic Sciences and Technology of China, Chengdu, People's Republic of China